ChemComm

FEATURE ARTICLE

View Article Online
View Journal | View Issue

Cite this: *Chem. Commun.*, 2017, 53, 6685

Quantification of f-element covalency through analysis of the electron density: insights from simulation

A. Kerridge

Received 6th February 2017,
Accepted 15th May 2017

DOI: 10.1039/c7cc00962c

rsc.li/chemcomm

The electronic structure of f-element compounds is complex due to a combination of relativistic effects, strong electron correlation and weak crystal field environments. However, a quantitative understanding of bonding in these compounds is becoming increasingly technologically relevant. Recently, bonding interpretations based on analyses of the physically observable electronic density have gained popularity and, in this *Feature Article*, the utility of such density-based approaches is demonstrated. Application of Bader's Quantum Theory of Atoms in Molecules (QTAIM) is shown to elucidate many properties including bonding trends, orbital overlap and energy degeneracy-driven covalency, oxidation state identification and bond stability, demonstrating the increasingly important role that simulation and analysis play in the area of f-element bond characterisation.

1. Introduction

The f-elements, comprised of the lanthanide (Ln: Z = 57–71) and actinide (An: Z = 89–103) ions, play an increasingly important role in our lives.[1] The technological applications of the lanthanides are far-ranging: complexes of gadolinium (and to a lesser extent europium, terbium, dysprosium, thulium and ytterbium) are routinely used as contrast agents in magnetic resonance imaging,[2,3] and the optical properties of the lanthanides are exploited more broadly in energy efficient lighting components. Neodymium is the commonly used material in wind turbine magnets and the magnetic properties of other lanthanides, such as praseodymium, dysprosium and thulium, are exploited elsewhere, for example in consumer electronics and in hybrid electric vehicles. The latter also exploit the lanthanides in the context of rechargeable batteries, while vast quantities of ceria (CeO_2) is used in catalytic converters by the traditional automotive industry.[4]

In contrast, the majority of technological applications of the actinides are associated with uranium, which is integral to our current approaches to energy production *via* nuclear fission. The use of uranium in the nuclear power industry leads to the production of other radiotoxic actinides, primarily plutonium, but also the minor actinide (MA) elements, namely neptunium, americium and curium. Separation of neptunium from uranium in the PUREX (Plutonium Uranium Redox EXtraction) process can be problematic and, more broadly, storage of the minor actinides represents a significant health hazard, with their safe management requiring substantial economic commitment and research resources.[5] A developing strategy in the management of minor actinide-containing spent fuel is solvent extraction based SANEX (Selective ActiNide EXtraction) and TALSPEAK (Trivalent Actinide Lanthanide Separation by Phosphorus reagent Extraction from Aqueous Komplexation) processes which exploit differences in the thermodynamic stability of analogous Ln and MA complexes to effect separation of the two. It is believed that variation in the

Department of Chemistry, Faraday Building, Lancaster University, Lancaster, LA1 4YB, UK. E-mail: a.kerridge@lancaster.ac.uk; Web: akresearch.wordpress.com

A. Kerridge

Andy Kerridge is a Lecturer in the Department of Chemistry, Lancaster University. After obtaining his PhD in Physics with Professor Marshall Stoneham at University College London, he completed a post-doctoral position in the London Centre for Nanotechnology. He subsequently worked as a PDRA with Prof Nik Kaltsoyannis in the UCL Department of Chemistry, employing state of the art quantum chemical simulations to contemporary problems in f-element chemistry. Andy was awarded an EPSRC Career Acceleration Fellowship in 2011 and took up his current Lectureship in 2014. Working closely with experimentalists, his group applies quantitative simulation methods to characterise f-element bonding.

covalent contributions to bonding contributes to the effectiveness of this approach,[6] although conclusive evidence remains elusive.

Whilst uranium is the dominant actinide from a technological perspective, applications of other members of the series do exist. For example, plutonium is used in the thermoelectric generators which act as power sources for the deep-space Voyager, Curiosity and New Horizons probes, as well as finding utility in human pacemakers. Due to the scarcity of the isotope required for this technology (^{238}Pu), americium and curium are under consideration as alternatives. Americium also finds application in household smoke detectors, where sub-μg quantities are used as ionisation sources.

In addition to their technological relevance, the chemistry of the f-elements is fascinating from a fundamental science perspective: the lanthanides, which exhibit partial population of the high-angular momentum (l = 3) 4f shell, have intriguing magnetic properties that can be modulated by their ligand environments.[7] While lanthanide bonding can, with some notable exceptions,[8–12] be characterised as ionic in nature, actinide bonding is highly complex: compounds typically exhibit strong relativistic effects, substantial electron correlation and weak crystal fields. Combined, these phenomena result in a poorly-defined valence region in which the 5f, 6d and 7s shells may each play a role in bonding.[13] Intriguingly, the 6p shell, which is typically considered to be core-like, can also impact on bonding in a manner that is challenging to characterise.[14,15] Deepening our understanding of chemical bonding in complexes of the f-elements and quantifying the nature of this bonding is therefore at the forefront of current f-element research. Opportunities to experimentally investigate the nature of f-element bonding are, however, currently rather limited (see Section 2) and so quantum chemical simulation, combined with appropriate analysis, offers an important and accessible alternative.[16,17] In this *Feature Article*, recent computational progress into the characterisation of f-element bonding and quantitation of its covalent character is reported and contrasted with experimental advances.

Whilst the meaning of covalency is well-understood from a chemical perspective, there is no formal physical definition. However, from a quantum chemical perspective the manifestation of covalency can be considered in terms of perturbation theory.[18] In a molecular orbital description of electronic structure, the mixing of a formally metal-based orbital, $\varphi_{\mathrm{M}}(\mathbf{r})$, with a formally ligand-based orbital, $\varphi_{\mathrm{L}}(\mathbf{r})$, can be described in terms of a mixing parameter λ, defined as:

$$\lambda = \frac{H_{\mathrm{ML}}}{\Delta E_{\mathrm{ML}}} \qquad (1)$$

where H_{ML} is the Hamiltonian matrix element between the two orbitals and ΔE_{ML} is the energy difference between them. Covalency is pronounced when λ is large. This description immediately reveals two different mechanisms by which covalency can be realised. Firstly, *via* energetic near-degeneracy (*i.e.* small ΔE_{ML}), and secondly, *via* orbital overlap (*i.e.* large H_{ML}). These two manifestations can therefore be considered as degeneracy-driven and overlap-driven covalency, respectively (see Fig. 1), and it is important to recognise that only the latter would be expected to result in thermodynamic stabilisation of the bonding interaction due to electronic charge accumulation in the bonding region.

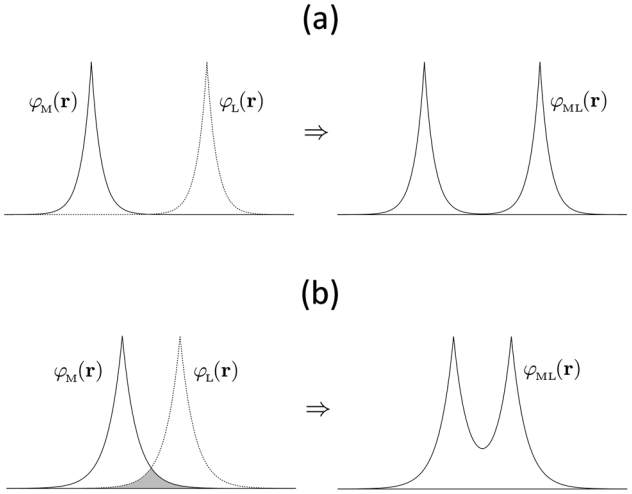

Fig. 1 Schematic of (a) degeneracy-driven and (b) overlap-driven covalent interactions.

2. Experimental measures of covalency

Numerous spectroscopic approaches have been employed in order to provide evidence of f-element covalency.[19] Variation in the relative intensity of photoionization cross-sections has allowed photoelectron spectroscopy (PES) to be employed as a probe of U(VI) and U(IV) 5f-orbital contributions to bonding,[20–22] whereas Mössbauer spectroscopy, which can be used to investigate the shielding of s-orbitals by valence orbitals with higher angular momenta, has been used to provide evidence of enhanced Np(IV) covalency in comparison to a Eu(III) analogue.[23] More recently, emission spectroscopy has been employed in the identification of unusual bonding in californium-containing compounds, interpreted as being due to Cf(III) 7p covalency.[24,25] Two-dimensional ^{1}H, ^{15}N-HMQC (Heteronuclear Multiple Quantum Coherence) Nuclear Magnetic Resonance (NMR) spectroscopy has been used to provide evidence for enhanced covalency in Am(III) compounds in comparison to Lu(III) and Sm(III) analogues,[26] whereas ^{77}Se and ^{125}Te NMR has provided evidence of U(VI) 5f-contributions to bonding.[27] Electron Paramagnetic Resonance spectroscopy (EPR) has been used to establish 5f contributions to bonding in several complexes of U(V)[28,29] and the application of pulsed-EPR has resulted in the quantification of spin-density present on organic ligands coordinating uranium and thorium centres.[30]

Perhaps the most widely-accepted current experimental measure of covalent contributions to f-element bonding comes in the form of X-Ray Absorption Spectroscopy (XAS). Pioneering work by Solomon and co-workers[31] established XAS a viable probe of transition metal covalency and this approach has been

extended to demonstrate covalent contributions to f-element bonding in uranyl (UO_2^{2+}),[32] U(IV) metallocene dichlorides,[33] Ce(IV) and U(IV) halides,[9,18] uranocene ($U(\eta^8\text{-}C_8C_8)_2$),[34] lanthanide sesquioxides[10] and Th(IV) hexacyanoferrate.[35]

Whilst XAS provides unparalleled spectroscopic insight into the nature of f-element bonding it is unable, as a stand-alone technique, to differentiate between degeneracy- and overlap-driven covalency since, in essence, it probes the metal contribution to formally ligand-based valence p-orbitals that may be present in both situations. Quantum chemical simulations, when appropriately analysed, are able to probe both degeneracy- and overlap-driven covalent interactions and are therefore able to provide increasingly relevant quantitative descriptions of f-element bonding.

3. Analysis of simulated electron structure

Computational molecular-orbital (MO) based simulation methods are focused on the (approximate) solution to the many-electron Schrödinger equation and, invariably, involve the construction of a model Hamiltonian. The eigenfunctions of this Hamiltonian are the (canonical) molecular orbitals. Each occupied MO can be thought of as a quantum mechanical description of a single pair of electrons in a chemical system, but this interpretation is only allowed under the independent particle approximation (IPA), whereby the total many-electron wavefunction can be written as an antisymmetrised product of the occupied MOs. The IPA typically provides a good approximation to the exact wavefunction, however there are numerous situations whereby the approximation breaks down. Structural environments in which this occurs include non-equilibrium geometries and transition states, whereas weak crystal field environments, degenerate ground-states and strong electron correlation provide examples with an electronic origin.

Analysis of simulated electron structure can be largely separated into two approaches: those based around analysis of molecular orbitals and those based around analysis of the electron density. Recently, both Kaltsoyannis and Dognon have provided comprehensive summaries of the application of such analysis methods to problems in f-element chemistry.[6,36] It should be noted that an alternative approach based on decomposition of the molecular energy into its contributing components, Energy Decomposition Analysis (EDA),[37–39] has also been successfully applied to f-element bonding.[40,41]

3.1 Orbital-based analyses

The simplest of the orbital-based analyses are based on direct examination of the canonical MOs. Such analyses are typically only used to provide qualitative bonding information, although quantitative data can be generated. Examples of this approach include Mulliken[42] and Löwdin[43] population analyses and Wiberg[44] and Mayer[45] bond order analyses.

Whilst computationally inexpensive, orbital-based analysis approaches are of limited utility. The set of occupied canonical MOs does not provide a unique description of electronic structure, since unitary transformations of this set leave the total energy of the system unchanged. Numerous localisation approaches including the Foster-Boys,[46] Edmiston-Ruedenberg[47] and Pipek-Mezey[48] procedures take advantage of this property, but from a quantitative perspective, orbital-based bonding analyses are prone to ambiguity.

3.2 Density-based analyses

The electron density, in contrast to the electronic wavefunction, is a physical observable and therefore represents a well-defined property to analyse. Numerous density-based approaches exist, including Hirshfeld,[49] natural bond orbital[50] (NBO) and electron localisation function[51,52] (ELF) analyses, however, in recent years, Bader's quantum theory of atoms in molecules[53] has gained increasing popularity due to its ability to probe multiple aspects of bonding in a coherent, quantitative and rigorous framework.

3.2.1 The quantum theory of atoms in molecules. The quantum theory of atoms in molecules (QTAIM) is based on the concept of a partitioning of a molecular system into a set of contiguous, space-filling atomic volumes. Each atomic volume is defined by a surface satisfying the zero-flux condition:

$$\nabla\rho(\mathbf{r})\cdot\mathbf{n}(\mathbf{r}) = 0 \qquad (2)$$

where $\rho(\mathbf{r})$ is the electron density and $\mathbf{n}(\mathbf{r})$ is a unit vector normal to the surface at the point $\mathbf{r}$. Analysis of the topology of the electron density reveals the set of critical points, *i.e.* points where the gradient in the density vanishes, $\nabla\rho(\mathbf{r}) = 0$. These critical points can be categorised into four types, depending on the curvature of the density at the point (see Table 1). The rank of the critical point, ω, gives the number of non-zero curvatures of $\rho(\mathbf{r})$ at that point, while the signature, σ, is the sum of the sign (±1) of each curvature. Each atomic volume, or basin (labelled Ω), contains exactly one nuclear critical point (NCP), at the position of a nucleus, and, as shown in Fig. 2a, this atomic partitioning of space is visually analogous to a space-filling model of a molecule.

Along with NCPs, bond, ring and cage critical points can be identified and, of these, the bond critical point (BCP) is of most relevance in quantifying bond character. A bond critical point exists if the line of minimum density between two atoms has its minimum point where the corresponding atomic basins share a common surface, since only then is the $\nabla\rho(\mathbf{r}) = 0$ condition satisfied. BCPs are most commonly employed to characterise the nature of a chemical interaction and a well-cited rule of thumb states that $\rho(\mathbf{r}) > 0.2$ a.u. with $\nabla^2\rho(\mathbf{r}) < 0$ is indicative of

Table 1 Characterisation of QTAIM-derived critical points in the electron density

Critical point	(ω, σ)	Character
Nuclear (NCP)	(3, −3)	Local maximum
Bond (BCP)	(3, −1)	1st-order saddle point
Ring (RCP)	(3, +1)	2nd-order saddle point
Cage (CCP)	(3, +3)	Local minimum

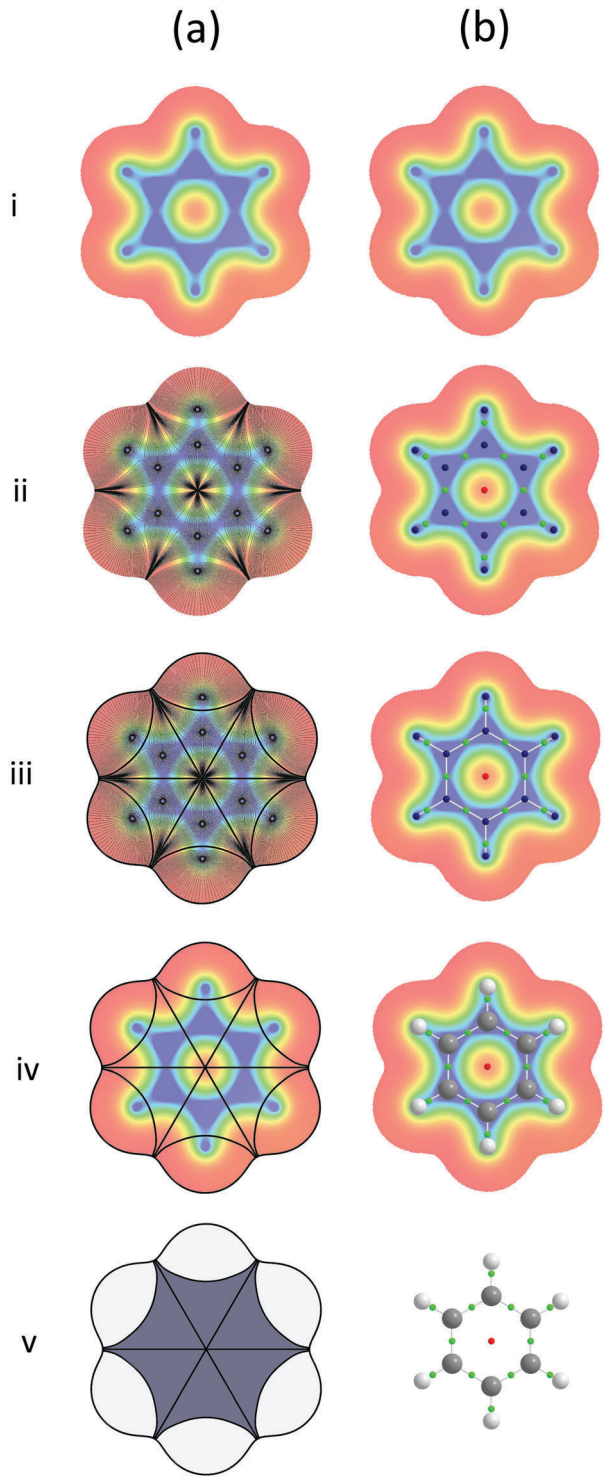

Fig. 2 The relationship between QTAIM and traditional molecular models, taking benzene, C_6H_6, as an example. (a(i)) $\rho(r)$; (ii) $\nabla\rho(r)$; (iii) $\nabla\rho(r)\cdot n(\mathbf{r}) = 0$; (iv) atomic basins; (v) space-filling analogue. (b(i)) $\rho(\mathbf{r})$; (ii) BCPs; (iii) molecular graph; (iv) NCPs replaced by spheres representing nuclei. (v) Ball-and-stick analogue.

an open-shell (*i.e.* covalent) interaction, whereas $\rho(\mathbf{r}) < 0.1$ a.u. with $\nabla^2\rho(\mathbf{r}) > 0$ represents a closed shell (*i.e.* ionic, van der Waals or hydrogen bonding) interaction. It should be noted, however, that there is no *a priori* reason to assume that this rule should hold for f-element bonding.

The lines of minimum density which join the BCPs to the NCPs are known as bond paths and the combination of critical points and bond paths together form the molecular graph of the system, which is visually analogous to the ball-and-stick model of a molecule, see Fig. 2b(v). Characterisation of a chemical system in this manner is a form of topological analysis.

In addition to providing analogies to traditional models of a molecule, QTAIM parameters give quantitative insight into the nature of chemical bonding. Integration over atomic basins allows quantification of the degree of electron sharing between neighbouring atoms, thereby providing insight into both degeneracy- and overlap-driven covalency. The value of the electron density at the BCP, ρ_{BCP}, along with its Laplacian, provides complementary data. ρ_{BCP} indicates the presence and degree of covalent character in the bond *via* a direct quantification of charge accumulation in the bonding region and hence provides a measure of overlap-driven covalency (*cf.* Fig. 1b). The ability of the QTAIM to interrogate both degeneracy- and overlap-driven covalency thus makes it ideally suited to contemporary problems in f-element bonding.

3.3 Bonding trends in the lanthanide and actinide series

Pioneering work by the Kaltsoyannis group represents some of the earliest applications of QTAIM analysis in f-element chemistry. Tassell and Kaltsoyannis investigated covalency in the organometallics $AnCp_4$ (Cp = η^5-C_5C_5) where An = Th–Cm.[54] Analysing densities generated using the density functional theory (DFT) approach employing the generalised gradient approximation (GGA) in the form of the PBE exchange–correlation functional, the authors found that, according to the magnitude of ρ_{BCP}, An–Cp bonding was highly ionic in character, with greater covalency found near the beginning of the series. This contrasted with Mulliken analysis which suggested increased f-orbital contribution to bonding MOs as the actinide series was traversed. Kirker and Kaltsoyannis performed related studies on $AnCp_3$ where An = Th–Cm, analysing densities generated using both the PBE and hybrid-GGA PBE0 exchange–correlation functionals. The authors came to the same conclusion,[55] namely that there is little appreciable charge accumulation in the An–Cp bonds and that what little charge density is present diminishes as the actinide series is traversed. Kerridge investigated the bonding in $AnCOT_2$ (COT = η^5-C_8C_8), where An = Th–Cm, using the complete-active-space self-consistent-field (CASSCF) methodology.[56] QTAIM analysis of CASSCF-derived densities again revealed a trend of diminishing covalency, as measured by the magnitude of ρ_{BCP}, as the series was traversed (see Fig. 3), with a plateau between Pa and Pu. Kerridge also investigated the delocalisation index, δ(An,C), a measure of the degree of electron-sharing between the actinide and carbon atoms, identifying a similar, though less pronounced trend, thereby demonstrating that in these systems, covalency was more overlap-driven in nature for An = Pa–Pu, as evidenced by ρ_{BCP}.

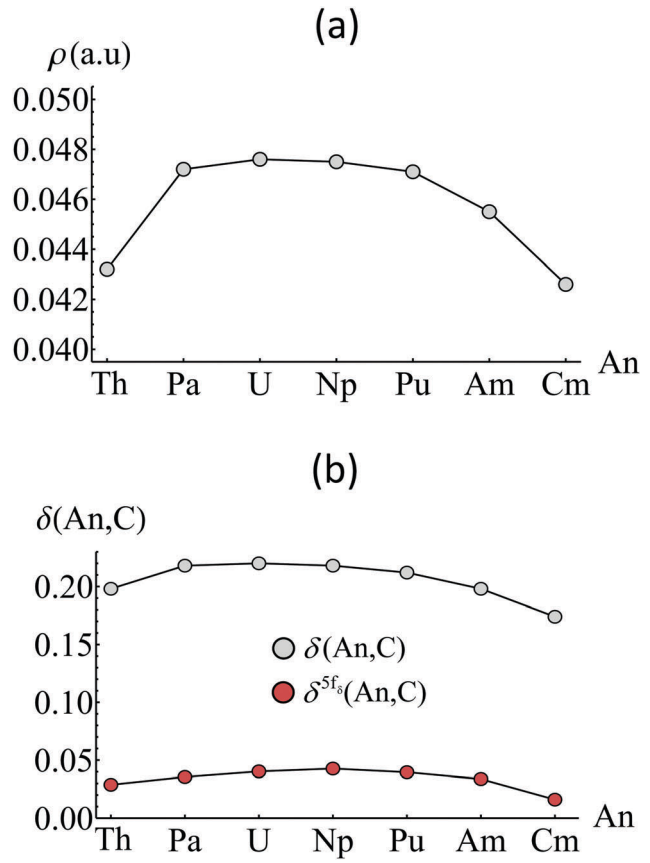

Fig. 3 Variation of (a) ρ_{BCP} and (b) δ(An,C) in $AnCOT_2$ when the An centred is varied. Adapted from ref. 56 (DOI: 10.1039/c3ra47088a) with permission from the Royal Society of Chemistry.

Table 2 Comparison of reported ρ_{BCP} values and their variation with respect to actinide species[54–56]

	An(III)Cp_3[a]	An(IV)Cp_4[a]	An(IV)COT_2[b]
Th	0.039	0.033	0.043
Pa	0.040	0.034	0.047
U	0.040	0.034	0.048
Np	0.039	0.033	0.048
Pu	0.038	0.032	0.047
Am	0.036	0.029	0.046
Cm	0.034	0.027	0.042

[a] PBE-derived densities. [b] CASSCF-derived densities. All values are in a.u.

Reported ρ_{BCP} values from these studies are summarised in Table 2. While all values are indicative of predominantly ionic interactions (recall that ρ_{BCP} is typically greater than 0.2 a.u. for pronounced covalent bond character), significant variation is found when the ligating species is altered. Interestingly, An interactions with the COT ligand are more covalent than those with the Cp ligand, with ρ_{BCP} values ~50% higher in the former. This is, in part, attributable to the higher charge density on the formally dianionic COT ligand which appears to contribute to the bonding interaction.

Beyond organometallic complexes, Wang *et al.* analysed PBE-derived densities of AnF_4, where An = Th–Cm: similarly to the above, they found larger ρ_{BCP} values between Pa and Pu, with the magnitude decreasing for later actinides.[58] Huang *et al.* investigated $[AnO_n]^{m+}$ (n = 1, 2; m = 0–2) where An = Th–Cm[59] and, in contrast to previous reports, found pronounced evidence for charge accumulation in the An–O bonds, reporting ρ_{BCP} values in excess of 0.2 a.u. and δ(An,O) values close to, and in many cases exceeding, 2. Despite these pronounced covalent interactions, The trend across the series mirrored that previously reported, with Pa, U, Np and Pu exhibiting more pronounced overlap-driven covalency.

The lanthanides are more readily classified as ionically bonded complexes and as a consequence less attention has been paid to Ln bond characterisation. The only systematic study in the literature is that of Fryer-Kanssen *et al.*, who investigated $[Ln(H_2O)_9]^{3+}$ and $[Ln(BTP)_3]^{3+}$ (BTP = bis(triazinyl)-pyridine) complexes with Ln = Ce–Lu.[57] As might be expected, topological analysis of densities generated using the hybrid-GGA exchange–correlation functionals B3LYP and BHLYP revealed low values of ρ_{BCP} in all cases and only small (<10%) variation as the series was traversed, indicative of predominantly ionic bonding with little dependence on the nature of the central ion, see Fig. 4.

3.4 Actinyl bonding

Uranyl, UO_2^{2+}, is the dominant form of uranium in the +6 oxidation state and is characterised by short strong U–O multiple bonds. Uranyl, along with its Pu analogue, plutonyl, were first investigated *via* QTAIM by Clark *et al.* in 2004, although topological properties were not reported.[60] QTAIM properties of the U–O bond have been reported by Vallet *et al.*[61] who found strongly covalent interactions with, for example, ρ_{BCP} = 0.38 a.u. and a delocalisation index δ(U,0) = 2.29 for densities generated using the hybrid-GGA B3LYP exchange–correlation functional. These results again demonstrate the presence of overlap-driven covalency. The authors also investigated the effect of equatorial complexation on the U–O bond and found that this resulted in reduced covalent character.

A related study by Di Pietro and Kerridge[62] found similar bonding characteristics: ρ_{BCP} = 0.364 a.u. and δ(An,C) = 2.19 for

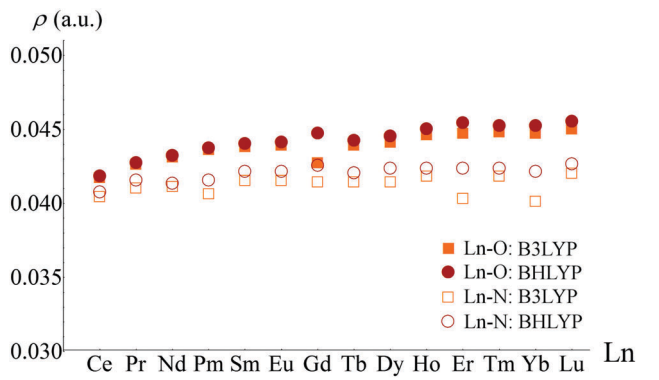

Fig. 4 Variation of ρ_{BCP} in Ln–O and Ln–N bonds of $[Ln(H_2O)_9]^{3+}$ and $[Ln(BTP)_3]^{3+}$, respectively. Adapted from ref. 57. Reprinted with permission from DOI: 10.1021/acs.inorgchem.6b00968. Copyright 2016 American Chemical Society.

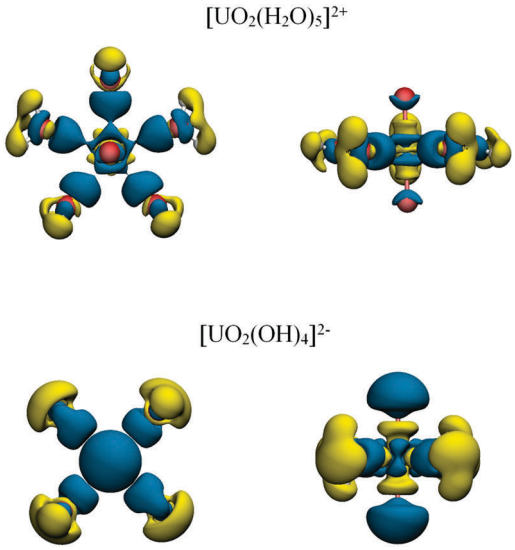

Fig. 5 Redistribution of electron density due to uranyl complexation by water and hydroxide. Blue and yellow regions indicate charge accumulation and depletion, respectively. Adapted from ref. 62. Reprinted with permission from DOI: 10.1021/acs.inorgchem.5b01219. Copyright 2016 American Chemical Society.

densities generated using the hybrid meta-GGA TPSSh exchange–correlation functional. The authors performed a detailed analysis of the effects of equatorial complexation on the electronic structure of the uranyl unit, concluding that equatorial complexation led to a localisation of electronic charge on the uranyl oxygen centres, reducing the covalent character of the U–O bond and consequently lengthening and weakening it. Charge localisation on the oxygen centres appeared to allow the uranium centre to instead donate charge into equatorial bonds. This quantitative description could also be qualitatively visualised, by investigating the change in charge density distribution induced by equatorial complexation (see Fig. 5).

Du *et al.* have analysed B3LYP-derived densities of plutonyl, PuO_2^{2+}, and found covalency of comparable magnitude to that in uranyl,[63] with ρ_{BCP} = 0.376 a.u. and δ(Pu,O) = 2.37, while equatorial complexation was found to be largely ionic in nature. This latter finding is in contrast to the results of Vallet *et al.* who found some degree of equatorial charge accumulation when uranyl was coordinated by peroxide and carbonate species.[61]

Brown *et al.* have investigated more exotic analogues of uranyl, where one axial oxygen is substituted by a heavier chalcogen, resulting in UOE^{2+}, with E = S or Se. While such analogues do not exist as isolated ions, they can be stabilised *via* equatorial ligation by, for example, bis(silyl)amide.[64] Analysis of PBE-derived densities revealed that substitution by a heavier chalcogen resulted in a reduction of U–O ρ_{BCP} values, although this reduction was not pronounced. U–E bonds, however, exhibited significantly less covalent character, with ρ_{BCP} values more than 50% lower than corresponding U–O values. This is presumably due to the softer, less electronegative S and Se species providing a poor bonding environment for the uranium centre, which is characterised as a hard acceptor.

3.5 Oxidation state dependency

Few systematic density-based studies investigating the dependency of covalent bond character on metal oxidation state exist. Beekmeyer and Kerridge analysed DFT-, RASSCF and- CASSCF-derived $[UCl_6]^{n-}$ (n = 0–3) densities[65] and determined that, while only weak covalency, as evidenced by ρ_{BCP} and δ(U,Cl) measures, was present, oxidation state dependence was pronounced, see Table 3. The authors found that, irrelevant of the simulation method used, covalent bond character was most pronounced in the highest (+6) oxidation state, with ρ_{BCP} values for the lowest (+3) some 60% lower. δ(U,Cl) values gave a similar, albeit less pronounced, trend. Interestingly, while ρ_{BCP} values showed little dependence on simulation methodology, it was found that DFT-derived densities gave consistently higher delocalisation indices, thereby demonstrating enhanced degeneracy-driven covalency without a corresponding increase of charge accumulation in the bond.

Huang *et al.* have investigated the +2 to +6 oxidation states in a series of actinide oxides, $[AnO_n]^{m+}$ (n = 1, 2; m = 0–2) where An = Th–Cm,[59] see Table 4. For uranium and heavier actinides, the same trend as found by Beekmeyer and Kerridge[65] was reported, whereas Th and Pa oxides were found to exhibit more complicated behaviour. Covalent bond character was found to be sensitive to the coordination environment of the actinide,

Table 3 QTAIM metrics of uranium hexachloride, $[UCl_6]^{n-}$ (n = 0–3), as a function of uranium oxidation state and simulation method. Data taken from ref. 65. All values are in a.u.

	Metric	CASSCF	RASSCF	B3LYP	PBE
U(VI)	ρ_{BCP}	0.105	0.102	0.099	0.096
	δ(U,Cl)	0.838	0.868	1.102	1.151
U(V)	ρ_{BCP}	0.086	0.084	0.082	0.081
	δ(U,Cl)	0.673	0.647	0.872	0.932
U(IV)	ρ_{BCP}	0.064	0.059	0.063	0.065
	δ(U,Cl)	0.482	0.442	0.633	0.619
U(III)	ρ_{BCP}	0.038	0.037	0.041	0.044
	δ(U,Cl)	0.324	0.300	0.432	0.487

Table 4 ρ_{BCP} and δ(An,O) values of actinide oxides, $[AnO_n]^{m+}$ (n = 1, 2; m = 0–2), as a function of actinide oxidation state, obtained from B3LYP-derived densities. δ(An,O) values are given in parentheses. Data taken from ref. 59. All values are in a.u.

	$[AnO_2]^{m+}$			$[AnO]^{m+}$		
	An(VI)	An(V)	An(IV)	An(IV)	An(III)	An(II)
Th	0.195	0.228	0.224	0.314	0.283	0.262
	(1.598)	(1.704)	(1.738)	(2.116)	(2.041)	(2.044)
Pa	0.288	0.314	0.288	0.336	0.287	0.284
	(2.046)	(2.031)	(2.053)	(2.228)	(2.031)	(2.157)
U	0.377	0.325	0.290	0.346	0.284	0.259
	(2.305)	(2.084)	(2.067)	(2.315)	(2.023)	(2.005)
Np	0.380	0.338	0.273	0.346	0.286	0.259
	(2.336)	(2.143)	(1.942)	(2.372)	(2.074)	(2.042)
Pu	0.387	0.347	0.270	0.335	0.285	0.257
	(2.363)	(2.182)	(1.921)	(2.417)	(2.097)	(2.061)
Am	0.385	0.339	0.254	0.282	0.283	0.242
	(2.360)	(2.175)	(1.864)	(2.248)	(2.079)	(2.011)
Cm	0.359	0.307	0.245	0.232	0.269	0.241
	(2.266)	(2.026)	(1.745)	(1.827)	(2.081)	(2.029)

with the individual bonds of the 2 : 1 complexes exhibiting less covalent character than analogous 1 : 1 complexes, although the cumulative amount of electron sharing was found to be higher in the former.

Whilst the +VI oxidation state of uranium is typically associated with the uranyl structural motif, important exceptions exist. Liddle and coworkers have reported the U(VI) terminal nitride $\{[U(N)(Tren^{TIPS})]\ (Tren^{TIPS} = N(CH_2CH_2NSi^iPr_3)_3\}^{3-}$, $^iPr = CH(CH_3)_2$) and, *via* analysis of the DFT-generated electron density revealed ρ_{BCP} = 0.391 a.u. for the strongly covalent U≡N triple bond,[66] a value comparable to that of analogous group 6 nitrides as well as the U–O_{yl} bond of uranyl. Reduction to U(V) significantly reduces this covalent character to ρ_{BCP} = 0.252 a.u., while the U=N double bond in the corresponding U(VI) imido complex exhibits ρ_{BCP} = 0.16 a.u.[67] Substitution of the amido group by phosphinidene and arsenidene again reduces the covalent character of the double bond, with reported values of $\rho_{BCP} \leq 0.08$ a.u.[68,69]

3.6 d- and f-shell contributions to covalency

Advantage can be taken of the high symmetry of some coordination complexes of the f-elements to resolve the d- and f-contributions to QTAIM metrics. Assuming the Müller approximation,[70] the delocalisation index $\delta(A,B)$ can be written as:

$$\delta(A,B) = \sum_{i,j} \sqrt{n_i}\sqrt{n_j} S_{ij}(A) S_{ij}(B) \quad (3)$$

where n_i is the occupation number of natural orbital i and $S_{ij}(A)$ is an overlap integral between orbitals i and j over the atomic basin Ω_A:

$$S_{ij} = \int_{\Omega_A} \varphi_i^*(\mathbf{r})\varphi_j(\mathbf{r})\mathrm{d}\mathbf{r} \quad (4)$$

Since the electron density, $\rho(\mathbf{r})$, must have the same symmetry as the complex, so must the atomic basin of the central ion, Ω_{An}. Overlap integrals over Ω_{An} are then only non-zero when $\varphi_i(\mathbf{r})$ and $\varphi_j(\mathbf{r})$ span the same irreducible representation (irrep) of the point group to which the molecule belongs. If this point group contains the inversion operation, *i.e.* $f(x,y,z) = f(-x,-y,-z)$, then the atomic d-shells span gerade irreps, the f-shells span ungerade irreps and the delocalisation index between the An centre and a coordinating species can be decomposed into gerade and ungerade components, thereby resolving the d- and f-contributions. An example of the atomic basin of U in UCl_6, which has O_h (and therefore inversion) symmetry, is given in Fig. 6.

Kerridge has used density-based analysis to investigate the d_δ and f_δ contributions to metal–ligand bonding in $AnCOT_2$, where An = Th–Cm.[56] Although it was found that the gerade (d_δ) contribution was of greater magnitude than that of the ungerade (f_δ) component in each complex, the variation in the total contribution was mirrored by the ungerade component, and was indicative of a reduction as the An series is traversed, commensurate with the 5f shell becoming increasingly compact and core-like.

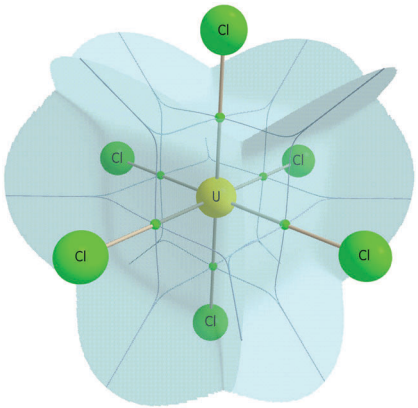

Fig. 6 The atomic basin, Ω_U, of the uranium centre in UCl_6, exhibiting O_h symmetry. Figure reproduced from ref. 65 (DOI:10.3390/inorganics3040482).

Beekmeyer and Kerridge have performed the same analysis to identify $(n + 1)$d and nf bonding contributions in $[MCl_6]^{n-}$, where M = Ce and U.[65] Comparing DFT to RASSCF/CASSCF generated densities, they found that the former gave delocalisation indices consistently higher than the latter. However, the majority of this increase could be attributed to the ungerade (*i.e.* f-shell) contribution, while the (d-shell) gerade component was largely insensitive to the methodology used to simulate the densities (see Fig. 7). The authors suggested that this may be a manifestation of the self-interaction error[71] which is inherent to approximate DFT methodologies and would be expected to be more pronounced in more highly correlated systems such as the valence f-shell of actinides and lanthanides.

3.7 U-like covalency in Ce compounds

In contrast to the trivalent lanthanides, which can be almost exclusively classified as exhibiting ionic bonding, recent studies have shown that compounds of cerium, the only lanthanide with an accessible tetravalent oxidation state, can exhibit covalent bond-character of comparable magnitude to that of U(IV) analogues.

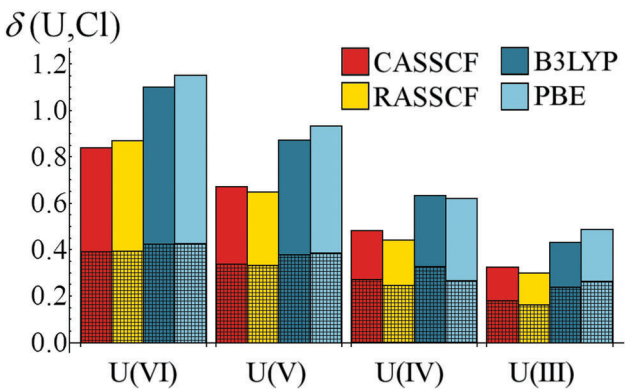

Fig. 7 Gerade and ungerade contributions to delocalisation indices in $[UCl_6]^{n-}$. Shaded regions represent gerade contributions. Figure reproduced from ref. 65 (DOI: 10.3390/inorganics3040482).

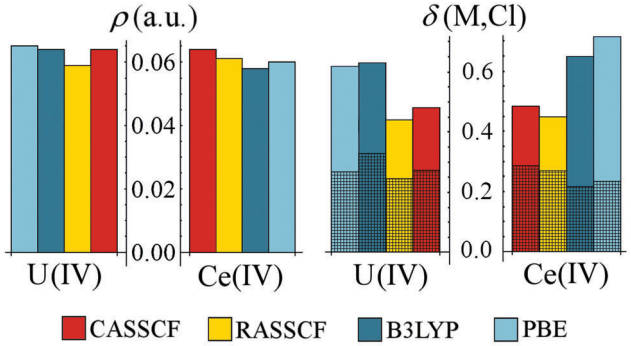

Fig. 8 Comparison of U–Cl and Ce–Cl covalency in $[MCl_6]^{2-}$. Figure adapted from ref. 65 (DOI: 10.3390/inorganics3040482).

Motivated by XAS studies indicating detectable covalency in Ce(IV) hexachloride,[9,18] Beekmeyer and Kerridge analysed DFT and CASSCF/RASSCF derived densities in order to quantify the covalency in this compound, along with its uranium analogue.[65] Remarkably, the magnitude of Ce and U covalency, as evidenced by ρ_{BCP} and δ(M,Cl), was almost identical, see Fig. 8. Similar behaviour was found in the carbene complexes M(BIPM^{TMS})-(ODipp)$_2$ (M = Ce, U, Th; BIPM^{TMS} = C(PPh$_2$NSiMe$_3$)$_2$; Dipp = C$_6$H$_3$-2,6-iPr$_2$) by Gregson *et al.*,[11] where the unusually short Ce-C double bond[72] was explained in terms of Ce–C covalency of a similar level to that of the U complex, a degree of covalency not present in the Th analogue. The ordering of covalency, Ce ~ U > Th, was reproduced in experimental exchange reactions with MCl salts. Building on this work, the related bis-carbene M(BIPM^{TMS})$_2$ (M = Ce, U, Th) complexes were synthesized by the same group.[12] The Ce complex exhibits one of the shortest reported Ce–C bond lengths, and represents the first evidence of the inverse-trans-influence (ITI) in tetravalent f-element chemistry. Analysis of CASSCF-derived densities again revealed Ce-covalency to be of the same magnitude as that found in the U–C bond, and the ellipticity of the density at the M–C BCP was indicative of double-bond character.

More recently, Damon *et al.* have reported a Ce(IV) oxo complex with pronounced covalent bond character.[73] Based on analysis of the PBE-derived density, a ρ_{BCP} value of 0.196 a.u. was found for the Ce–O bond. This is the largest reported value for a Ce complex in the literature, and is extremely close to the analogous U–O value of 0.199 a.u.

3.8 Correlating covalency with bond strength

Whilst a degree of covalent bond character can be identified in many complexes of the f-elements, relating this to bond strength is a challenging problem, since many other factors including, but not limited to, sterics and electrostatics, contribute to bond stability. Huang *et al.* have shown that bond strength is closely correlated to the degree of charge transfer upon complexation, as measured by analysis of QTAIM-derived charges.[59] Di Pietro and Kerridge have investigated the weakening of axial uranyl bonds to equatorial complexation, and find a strong correlation between axial vibrational frequencies and equatorial QTAIM parameters, see Fig. 9, indicating that it

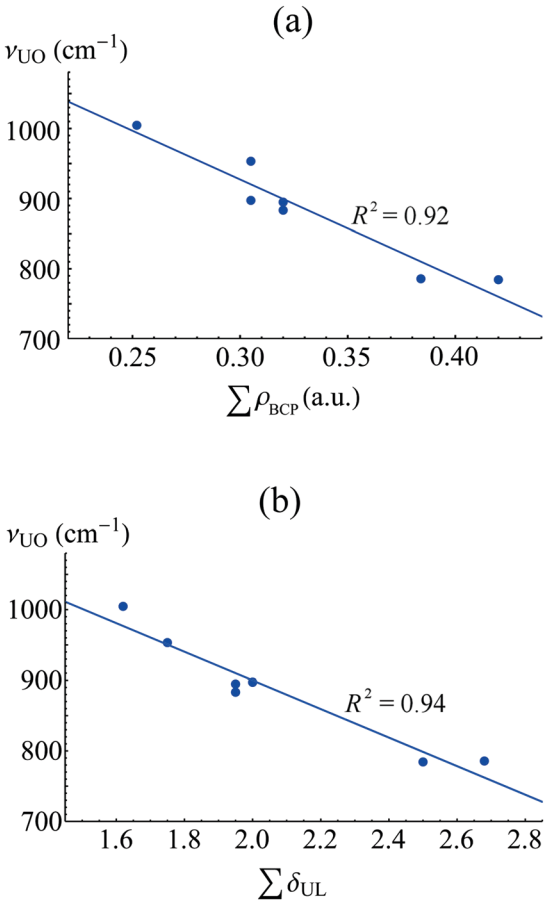

Fig. 9 Correlation between equatorial bond covalency, as measured by ρ_{BCP} and δ(U,L), and axial vibrational frequencies, for a series of actinyl complexes. Adapted from ref. 62. Reprinted with permission from DOI: 10.1021/acs.inorgchem.5b01219. Copyright 2016 American Chemical Society.

may be possible to probe equatorial bond covalency in related systems using standard spectroscopic techniques.

Fryer-Kanssen *et al.* have investigated the relationship between metal–ligand bond covalency and complex stability in

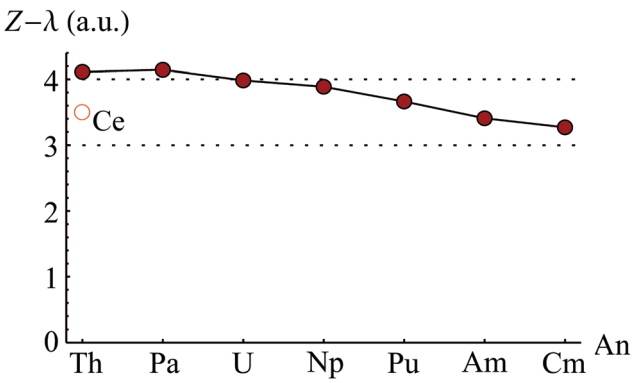

Fig. 10 QTAIM-derived oxidation state for the An centre in AnCOT$_2$. Adapted from ref. 56 (DOI: 10.1039/c3ra47088a) with permission from the Royal Society of Chemistry.

Table 5 QTAIM-derived oxidation states, OS_M, for a selection of f-element complexes

Complex	Formal OS	OS_M
UO_2L_n[80–82]	+6	+5.62–+6.12
$[UCl_6]^{n-}$ (n = 0–3)[65]	+6, +5, +4, +3	+5.75, +5.12, +4.25, +3.38
$An(E_2PL_2)_4$ (An = Th; U, E = S, Se; L= ^{t}Bu, ^{i}Pr)[83]	+4	+4.15–+4.29
$M(BIPM^{TMS})(ODipp)_2$ (M = Ce, Th, U)[11]	+4	+4.26–+4.39
$M(BIPM^{TMS})_2$ (M = Ce, Th, U)[12]	+4	+4.17–+4.34
$\{Th\text{-}(Cp'')_3\}_2(\mu\text{-}\eta^1\text{:}\eta^1\text{-}P_4)$,[84] $\{Th(Cp''')_2[\kappa_2\text{-}O_2C\{C_5H_3\text{-}3,3'\text{-}(SiMe_3)_2\}]\}_2(\mu\text{-}\kappa_2\text{:}\kappa_2\text{-}C_2O_4)$,[85] $[\{Th(Cp'')_3\}_2\{m\text{-}(NC_5H_4)_2\}]$, $\{Th(Cp'')_3\}_2\{m\text{-}(NC_5H_5)_2\}$[86] ($Cp''$ = $\{C_5H_3(SiMe_3)_2\text{-}1,3\}$)	+4	+4.20–+4.32
$[CeCl_6]^{n-}$ (n = 2,3)[65]	+4, +3	+4.23, +3.29
$[MBTP_3]^{3+}$ (M = Eu, Gd, Am, Cm)[57]	+3	+3.31–+3.50

$[M(BTP)_3]^{3+}$ complexes with M = Ln, Am, Cm.[57] They considered the exchange reaction:

$$[An(H_2O)_9]^{3+} + [Ln(BTP)_3]^{3+} \rightarrow [Ln(H_2O)_9]^{3+} + [An(BTP)_3]^{3+}$$

and, in agreement with previous energetic studies,[74–78] found evidence for the relative stability of $[An(BTP)_3]^{3+}$ over the Ln analogues. While An covalency was found to be higher in both the aquo and BTP complexes, the relative increase was larger in the latter, providing indirect evidence for covalent bond stabilisation in the An complex. It is worth noting here that a study demonstrating enhanced covalency in an Am complex when compared to a Nd analogue was amongst the first applications of QTAIM in f-element chemistry to be reported.[79]

3.9 Oxidation state identification

The formal oxidation state of a metal centre in a coordination complex is defined by assuming that any metal charge involved in a bonding interaction is donated entirely to the ligands. This definition lends itself to analysis *via* the QTAIM, since the electronic population of the atomic basin Ω_A, $N(A)$, can be defined in terms of the localisation and delocalisation indices, $\lambda(A)$ and $\delta(A,X)$:

$$N(A) = \lambda(A) + \frac{1}{2}\sum_{X \neq A}\delta(A,X) \quad (5)$$

Here, the localisation index $\lambda(A)$ provides a measure of the number of electrons localised on the atomic centre A. Therefore, a QTAIM metric of oxidation state can be defined by comparing $\lambda(A)$ to the atomic number of the atom in question, *i.e.*

$$OS_A = Z_A - \lambda(A) \quad (6)$$

Kerridge has applied this metric to a series of actinocenes, $AnCOT_2$, where An = Th–Cm.[56] In the actinocenes, the formal oxidation state of the An ion is +4, however this oxidation state becomes increasingly unstable as the series is traversed. Analysing RASSCF-derived densities, Kerridge demonstrated that QTAIM does indeed identify the +4 oxidation state for the early actinides, but OS_{An} drops to approximately +3 for the later actinides Am and Cm, see Fig. 10.

The question of oxidation state in cerocene, $CeCOT_2$, has been the subject of debate for several decades. Originally characterised as a Ce(IV) compound,[87–89] XANES spectroscopy[90] and *ab initio* calculations[91] supported an alternative interpretation, namely that the complex exhibits a multiconfigurational ground state with ~80% Ce(III) character. This surprising result was investigated by the Kaltsoyannis group,[92,93] who reported that the assignment of oxidation state based on configurational admixture was ambiguous. As a result of density based analysis, the authors assigned a +4 oxidation state, but noted significant charge delocalisation which could account for the reported XANES data. These apparently contradictory interpretations have since been shown to both be valid,[94] and Kerridge has calculated OS_{Ce} to be +3.500 based on analysis of a CASSCF-derived density.[95]

Table 5 summarises QTAIM-derived oxidation states for a number of simulated compounds. While in all cases rounding these values to the nearest integer yields the formal oxidation state, it remains to be demonstrated if this approach is applicable across the periodic table.

4. Conclusions

In this *Feature Article*, the utility of Bader's Quantum Theory of Atoms in Molecules (QTAIM) in the understanding of bonding in complexes of the f-elements has been considered and discussed. While significant use of this methodology in the f-element community has only occurred in the last few years, it is already allowing us to quantitatively probe heavy-element bonding at an unprecedented level of detail.

Like any analysis method, QTAIM is imperfect, in the sense that it does not always align with our chemical intuition, and may not reproduce all experimentally observed trends (although it should be borne in mind that an analytical method is only as good as the data to which it is applied). However, QTAIM provides a robust, rigorous, unambiguous, quantitative framework in which to interpret simulation and, occasionally, experimental[96,97] results. It's applicability to data generated using a variety of simulation methods allows for the straightforward comparison of different systems, a key strength. Perhaps the most important aspect of this (and related) analysis methods though is the fact that they are based on a physical observable, the electron density. This makes any prediction derived from this analysis empirically falsifiable, in principle at least. Few, if any, alternative methods offer such a promise.

Already-realised applications of QTAIM in f-element chemistry include the quantification and nature of bond-covalency and stability, oxidation state identification, and similarities/differences in lanthanide and actinide bonding. Potential future developments might include the ability to analyse spin–orbit

coupled densities and more importantly, a rigorous approach to energy decomposition. While a framework for such energy decomposition exists, the Interacting Quantum Atom (IQA) approach of Blanco *et al.*,[98] current implementations are not generally applicable to all exchange–correlation functionals, or to relativistic Hamiltonians. It is the author's belief that as familiarity with the methodology increases, so these developments will be achieved, more applications will be identified, and our understanding of the fundamental properties of f-element bonding will deepen.

Acknowledgements

AK thanks the Engineering and Physical Sciences Research Council for the award of a Career Acceleration Fellowship (EP/J002208/1; EP/J002208/2). AK thanks UCL, Lancaster University and the Nuclear Decommissioning Authority for funding.

Notes and references

1 J.-C. G. Bünzli, *J. Coord. Chem.*, 2014, **67**, 3706–3733.
2 K. N. Raymond and V. C. Pierre, *Bioconjugate Chem.*, 2005, **16**, 3–8.
3 M. W. Villaraza, A. J. L. Bumb and A. Brechbiel, *Chem. Rev.*, 2010, **110**, 2921–2959.
4 L. S. Natrajan and M. H. L. Paden, in *RSC Green Chemistry 22: Element Recovery and Sustainability*, ed. A. J. Hunt, Royal Society of Chemistry, London, 2013, pp. 140–184.
5 R. C. Ewing, *Nat. Mater.*, 2015, **14**, 252–257.
6 N. Kaltsoyannis, *Inorg. Chem.*, 2013, **52**, 3407–3413.
7 D. N. Woodruff, R. E. P. Winpenny and R. A. Layfield, *Chem. Rev.*, 2013, **113**, 5110–5148.
8 S. G. Minasian, J. L. Krinsky and J. Arnold, *Chem. – Eur. J.*, 2011, **17**, 12234–12245.
9 M. W. Löble, J. M. Keith, A. B. Altman, S. C. E. Stieber, E. R. Batista, K. S. Boland, S. D. Conradson, D. L. Clark, J. Lezama Pacheco, S. A. Kozimor, R. L. Martin, S. G. Minasian, A. C. Olson, B. L. Scott, D. K. Shuh, T. Tyliszczak, M. P. Wilkerson and R. A. Zehnder, *J. Am. Chem. Soc.*, 2015, **137**, 2506–2523.
10 A. B. Altman, J. I. Pacold, J. Wang, W. W. Lukens and S. G. Minasian, *Dalton Trans.*, 2016, **45**, 9948–9961.
11 M. Gregson, E. Lu, F. Tuna, E. J. L. McInnes, C. Hennig, A. C. Scheinost, J. McMaster, W. Lewis, A. J. Blake, A. Kerridge and S. Liddle, *Chem. Sci.*, 2016, **7**, 3286–3297.
12 M. Gregson, E. Lu, D. Mills, F. Tuna, E. McInnes, C. Hennig, A. Scheinost, J. McMaster, W. Lewis, A. Blake, A. Kerridge and S. T. Liddle, *Nat. Commun.*, 2017, **8**, 14137.
13 N. Kaltsoyannis, P. J. Hay, J. Li, J.-P. Blaudeau and B. E. Bursten, in *The Chemistry of the Actinide and Transactinide Elements*, ed. L. R. Morss, N. M. Edelstein, J. Fuger and J. J. Katz, Springer, Dordrecht, The Netherlands, 3rd edn, 2006, pp. 1893–2012.
14 R. G. Denning, *J. Phys. Chem. A*, 2007, **111**, 4125–4143.
15 E. O'Grady and N. Kaltsoyannis, *J. Chem. Soc., Dalton Trans.*, 2002, 1233–1239.
16 *Computational Methods in Lanthanide and Actinide Chemistry*, ed. M. Dolg, John Wiley & Sons Ltd, Chichester, 2015.
17 C. E. Kefalidis, L. Castro, L. Perrin, I. Del Rosal and L. Maron, *Chem. Soc. Rev.*, 2016, **45**, 2516–2543.
18 S. G. Minasian, J. M. Keith, E. R. Batista, K. S. Boland, D. L. Clark, S. D. Conradson, S. A. Kozimor, R. L. Martin, D. E. Schwarz, D. K. Shuh, G. L. Wagner, M. P. Wilkerson, L. E. Wolfsberg and P. Yang, *J. Am. Chem. Soc.*, 2012, **134**, 5586–5597.
19 M. L. Neidig, D. L. Clark and R. L. Martin, *Coord. Chem. Rev.*, 2013, **257**, 394–406.
20 B. W. Veal, D. J. Lam, W. T. Carnall and H. R. Hoekstra, *Phys. Rev. B: Solid State*, 1975, **12**, 5651–5663.
21 J. P. Clark and J. C. Green, *Dalton Trans.*, 1977, 505–508.
22 J. G. Brennan, J. C. Green and C. M. Redfern, *J. Am. Chem. Soc.*, 1989, **111**, 2373–2377.
23 G. M. Kalvius, *J. Less-Common Met.*, 1986, 353–378.
24 M. J. Polinski, E. B. Garner, R. Maurice, N. Planas, J. T. Stritzinger, T. G. Parker, J. N. Cross, T. D. Green, E. V. Alekseev, S. M. Van Cleve, W. Depmeier, L. Gagliardi, M. Shatruk, K. L. Knappenberger, G. Liu, S. Skanthakumar, L. Soderholm, D. A. Dixon and T. E. Albrecht-Schmitt, *Nat. Chem.*, 2014, **6**, 387–392.
25 S. K. Cary, M. Vasiliu, R. E. Baumbach, J. T. Stritzinger, T. D. Green, K. Diefenbach, J. N. Cross, K. L. Knappenberger, G. Liu, M. A. Silver, A. E. DePrince, M. J. Polinski, S. M. Van Cleve, J. H. House, N. Kikugawa, A. Gallagher, A. A. Arico, D. A. Dixon and T. E. Albrecht-Schmitt, *Nat. Commun.*, 2015, **6**, 6827.
26 C. Adam, P. Kaden, B. B. Beele, U. Müllich, S. Trumm, A. Geist, P. J. Panak and M. A. Denecke, *Dalton Trans.*, 2013, **42**, 14068–14074.
27 D. E. Smiles, G. Wu, P. Hrobárik and T. W. Hayton, *J. Am. Chem. Soc.*, 2016, **138**, 814–825.
28 L. A. Seaman, G. Wu, N. Edelstein, W. W. Lukens, N. Magnani and T. W. Hayton, *J. Am. Chem. Soc.*, 2012, **134**, 4931–4940.
29 W. W. Lukens, N. M. Edelstein, N. Magnani, T. W. Hayton, S. Fortier and L. A. Seaman, *J. Am. Chem. Soc.*, 2013, **135**, 10742–10754.
30 A. Formanuik, A. Ariciu, F. Ortu, R. Beekmeyer, A. Kerridge, F. Tuna, E. J. L. Mcinnes and D. P. Mills, *Nat. Chem.*, 2017, **9**, 578–583.
31 E. I. Solomon, B. Hedman, K. O. Hodgson, A. Dey and R. K. Szilagyi, *Coord. Chem. Rev.*, 2005, **249**, 97–129.
32 R. G. Denning, J. C. Green, T. E. Hutchings, C. Dallera, A. Tagliaferri, K. Giarda, N. B. Brookes and L. Braicovich, *J. Chem. Phys.*, 2002, **117**, 8008–8020.
33 S. A. Kozimor, P. Yang, E. R. Batista, K. S. Boland, C. J. Burns, D. L. Clark, S. D. Conradson, R. L. Martin, M. P. Wilkerson and L. E. Wolfsberg, *J. Am. Chem. Soc.*, 2009, **131**, 12125–12136.
34 S. G. Minasian, J. M. Keith, E. R. Batista, K. S. Boland, D. L. Clark, S. A. Kozimor, R. L. Martin, D. K. Shuh and T. Tyliszczak, *Chem. Sci.*, 2014, **5**, 351.
35 T. Dumas, D. Guillaumont, C. Fillaux, A. Scheinost, P. Moisy, S. Petit, D. K. Shuh, T. Tyliszczak and C. Den Auwer, *Phys. Chem. Chem. Phys.*, 2016, **18**, 2887–2895.
36 J.-P. Dognon, *Coord. Chem. Rev.*, 2014, **266–267**, 110–122.
37 T. Ziegler and A. Rauk, *Inorg. Chem.*, 1979, **18**, 1558–1565.
38 T. Ziegler and A. Rauk, *Inorg. Chem.*, 1979, **18**, 1755–1759.
39 G. Frenking and F. M. Bickelhaup, in *The Chemical Bond: Fundamental Aspects of Chemical Bonding*, ed. G. Frenking and S. Shaik, Wiley-VCH Verlag GmbH & Co. KGaA, Weinheim, 2014.
40 G. Cavigliasso and N. Kaltsoyannis, *Inorg. Chem.*, 2007, **46**, 3557–3565.
41 J.-P. Dognon, C. Clavaguéra and P. Pyykkö, *Angew. Chem., Int. Ed. Engl.*, 2007, **46**, 1427–1430.
42 R. S. Mulliken, *J. Chem. Phys.*, 1955, **23**, 1833.
43 P.-O. Löwdin, *J. Chem. Phys.*, 1950, **18**, 365–375.
44 K. B. Wiberg, *Tetrahedron*, 1968, **24**, 1083–1096.
45 I. Mayer, *J. Comput. Chem.*, 2007, **28**, 204–221.
46 J. M. Foster and S. F. Boys, *Rev. Mod. Phys.*, 1960, **32**, 300–302.
47 C. Edmiston and K. Ruedenberg, *Rev. Mod. Phys.*, 1963, **35**, 457–465.
48 J. Pipek and P. G. Mezey, *J. Chem. Phys.*, 1989, **90**, 4916–4926.
49 M. A. Spackman and P. G. Byrom, *Chem. Phys. Lett.*, 1997, **267**, 215–220.
50 A. E. Reed, R. B. Weinstock and F. Weinhold, *J. Chem. Phys.*, 1985, **83**, 735–746.
51 A. D. Becke and K. E. Edgecombe, *J. Chem. Phys.*, 1990, **92**, 5397.
52 A. Savin, A. D. Becke, J. Flad, R. Nesper, H. Preuss and H. G. von Schnering, *Angew. Chem., Int. Ed.*, 1991, **30**, 409–412.
53 R. F. W. Bader, *Atoms in Molecules: A Quantum Theory*, Oxford University Press, Oxford, 1990.
54 M. J. Tassell and N. Kaltsoyannis, *Dalton Trans.*, 2010, **39**, 6576–6588.
55 I. Kirker and N. Kaltsoyannis, *Dalton Trans.*, 2011, **40**, 124–131.
56 A. Kerridge, *RSC Adv.*, 2014, **4**, 12078–12086.
57 I. Fryer-Kanssen, J. Austin and A. Kerridge, *Inorg. Chem.*, 2016, **55**, 10034–10042.
58 C. Wang, C. Cheng, J. Su and P. Huai, *Mol. Phys.*, 2015, **113**, 3450–3458.
59 Q.-R. Huang, J. R. Kingham and N. Kaltsoyannis, *Dalton Trans.*, 2015, **44**, 2554–2566.
60 A. E. Clark, J. L. Sonnenberg, P. J. Hay and R. L. Martin, *J. Chem. Phys.*, 2004, **121**, 2563–2570.

61 V. Vallet, U. Wahlgren and I. Grenthe, *J. Phys. Chem. A*, 2012, **116**, 12373–12380.
62 P. Di Pietro and A. Kerridge, *Inorg. Chem.*, 2016, **55**, 573–583.
63 J. Du, X. Sun and G. Jiang, *Int. J. Mol. Sci.*, 2016, **17**, 1–14.
64 J. L. Brown, S. Fortier, G. Wu, N. Kaltsoyannis and T. W. Hayton, *J. Am. Chem. Soc.*, 2013, **135**, 5352–5355.
65 R. Beekmeyer and A. Kerridge, *Inorganics*, 2015, **3**, 482–499.
66 D. M. King, F. Tuna, E. J. L. McInnes, J. McMaster, W. Lewis, A. J. Blake and S. T. Liddle, *Nat. Chem.*, 2013, **5**, 482–488.
67 D. M. King, J. Mcmaster, F. Tuna, E. J. L. Mcinnes, W. Lewis, A. J. Blake and S. T. Liddle, *J. Am. Chem. Soc.*, 2014, **136**, 5619–5622.
68 B. M. Gardner, G. Balázs, M. Scheer, F. Tuna, E. J. L. McInnes, J. McMaster, W. Lewis, A. J. Blake and S. T. Liddle, *Angew. Chem., Int. Ed.*, 2014, **53**, 4484–4488.
69 B. M. Gardner, G. Balázs, M. Scheer, F. Tuna, E. J. L. McInnes, J. McMaster, W. Lewis, A. J. Blake and S. T. Liddle, *Nat. Chem.*, 2015, **7**, 582–590.
70 A. M. K. Müller, *Phys. Lett. A*, 1984, **105**, 446–452.
71 V. Polo, E. Kraka and D. Cremer, *Mol. Phys.*, 2002, **100**, 1771–1790.
72 M. Gregson, E. Lu, J. McMaster, W. Lewis, A. J. Blake and S. T. Liddle, *Angew. Chem., Int. Ed. Engl.*, 2013, **52**, 13016–13019.
73 P. L. Damon, G. Wu, N. Kaltsoyannis and T. W. Hayton, *J. Am. Chem. Soc.*, 2016, **138**, 12743–12746.
74 M. Trumm, B. Schimmelpfennig and A. Geist, *Nukleonika*, 2015, **60**, 847–851.
75 J. Lan, W. Shi, L. Yuan, Y. Zhao, J. Li and Z. Chai, *Inorg. Chem.*, 2011, **50**, 9230–9237.
76 J. H. Lan, W. Q. Shi, L. Y. Yuan, Y. X. Feng, Y. L. Zhao and Z. F. Chai, *J. Phys. Chem. A*, 2012, **116**, 504–511.
77 Y. Yang, J. Liu, L. Yang, K. Li, H. Zhang, S. Luo and L. Rao, *Dalton Trans.*, 2015, 8959–8970.
78 M. Trumm and B. Schimmelpfennig, *Mol. Phys.*, 2016, **114**, 876–883.
79 L. Petit, L. Joubert, P. Maldivi and C. Adamo, *J. Am. Chem. Soc.*, 2006, **128**, 2190–2191.
80 P. Di Pietro and A. Kerridge, *Inorg. Chem.*, 2016, **55**, 573–583.
81 P. Di Pietro and A. Kerridge, *Phys. Chem. Chem. Phys.*, 2016, **18**, 16830–16839.
82 S. D. Woodall, A. N. Swinburne, A. Kerridge, P. Di Pietro, C. Adam, P. Kaden and L. S. Natrajan, *Chem. Commun.*, 2015, **51**, 5402–5405.
83 A. C. Behrle, A. Kerridge and J. R. Walensky, *Inorg. Chem.*, 2015, **54**, 11625–11636.
84 A. Formanuik, F. Ortu, R. Beekmeyer, A. Kerridge, R. W. Adams and D. P. Mills, *Dalton Trans.*, 2016, **45**, 2390–2393.
85 A. Formanuik, F. Ortu, C. J. Inman, A. Kerridge, L. Castro, L. Maron and D. P. Mills, *Chem. – Eur. J.*, 2016, **22**, 17976–17979.
86 A. Formanuik, F. Ortu, J. Liu, L. Nodaraki, F. Tuna, A. Kerridge and D. P. Mills, *Chem. – Eur. J.*, 2017, **23**, 2290–2293.
87 A. Streitwieser, S. A. Kinsley, J. T. Rigsbee, I. L. Fragala, E. Ciliberto and N. Rosch, *J. Am. Chem. Soc.*, 1985, **107**, 7786–7788.
88 K. N. Raymond and C. W. Eigenbrot, *Acc. Chem. Res.*, 1980, **13**, 276–283.
89 A. Streitwieser, S. A. Kinsley, C. H. Jenson and J. T. Rigsbee, *Organometallics*, 2004, **23**, 5169–5175.
90 C. Booth, M. Walter, M. Daniel, W. Lukens and R. Andersen, *Phys. Rev. Lett.*, 2005, **95**, 267202.
91 M. Dolg, P. Fulde, W. Küchle, C.-S. Neumann and H. Stoll, *J. Chem. Phys.*, 1991, **94**, 3011.
92 A. Kerridge, R. Coates and N. Kaltsoyannis, *J. Phys. Chem. A*, 2009, **113**, 2896–2905.
93 A. Kerridge and N. Kaltsoyannis, *C. R. Chim.*, 2010, **13**, 853–859.
94 O. Mooßen and M. Dolg, *Chem. Phys. Lett.*, 2014, **594**, 47–50.
95 A. Kerridge, *Dalton Trans.*, 2013, **42**, 16428–16436.
96 B. B. Iversen, F. K. Larsen, A. A. Pinkerton, A. Martin, A. Darovsky and P. A. Reynolds, *Acta Crystallogr., Sect. B: Struct. Sci.*, 1999, **55**, 363–374.
97 V. V. Zhurov, E. A. Zhurova, A. I. Stash, A. Pinkerton and A. Alan, *J. Phys. Chem. A*, 2011, **115**, 13016–13023.
98 M. A. Blanco, A. Martín Pendás and E. Francisco, *J. Chem. Theory Comput.*, 2005, **1**, 1096–1109.